Letters

Multioutput Isolated Power Supply With Selectable Constant Voltage and Constant Current Modes Based on Magnetic Coupling Resonance

Jiangui Li, Yinchong Peng, Longyang Wang, Zheyuan Guo, Guangbin Luo, Qinghe Si, and Ian Robertson, *Fellow, IEEE*

***Abstract*—A multioutput isolated power supply system based on magnetic coupling resonance (MOIPS-MCR) technology is proposed in this letter. It can not only selectively switch between constant voltage (CV) and constant current (CC) output modes at each receiver but also flexibly adjust the number of receivers, achieving high flexibility, high efficiency, and high security of power supply to multiple devices. The topology of the MOIPS-MCR was first introduced. Then, the output voltage and current expressions for each receiver in different modes were derived, and the principle of adjusting the number of receivers was introduced. An experimental prototype with two receivers was produced to validate the system's performance. Experimental results demonstrate that load-independent CV and CC modes at each receiver of the system and the flexible adjustment of the number of receivers can be achieved.**

***Index Terms*—Isolated power supply, load independent, magnetic coupling resonance, multiple output.**

I. Introduction

An ISOLATED power supply can transmit power while ensuring electrical isolation, featuring strong anti-interference ability and high security [1]. Traditional magnetic isolation power sources typically rely on transformers for power transmission and electrical isolation. In multiload application scenarios, high-frequency transformers with central taps are usually used to transmit power to multiple devices, which results in the number of output ports being determined during design and production, and it cannot be increased or decreased on demand during use [2].

Magnetic coupling resonance wireless power transmission technology utilizes the principle of resonance to transmit power between the transmitter and the receiver through magnetic field coupling, providing a solution for realizing a multioutput isolated power supply [3], [4], [5]. In [6], multiple independent constant voltage (CV) outputs were achieved by connecting several double-T resonant circuits to the common port at the receiver end. However, this method cannot achieve constant current (CC) output. In [7], three CV outputs were achieved by integrating two buck converters into a full-wave rectifier, offering lower cost but with a limited number of output ports. Cheng et al. [8] proposed an innovative wireless power transmission system with multiple CV outputs to provide high insulation levels for the gate drivers of multilevel converters. Nevertheless, this method also cannot achieve CC output. In [9] and [10], multiple CC outputs were proposed to provide power to the gate driver circuits in a multilevel converter. However, these methods cannot achieve CV output. A multioutput isolated power supply with switchable CV and CC output modes offers enhanced versatility, adapting flexibly to the requirements of various devices. However, the traditional implementation involves adding extra conversion circuits at the output terminal, thereby increasing the complexity of the system.

This letter proposes an isolated power supply system based on magnetic coupling resonance, achieving multiple CV and CC switching outputs. Compared with traditional systems, the proposed system allows flexible control of the mode (CV or CC) and the number of receivers. Therefore, it can be used to power different kinds of multiple gate drivers in multilevel converters. The basic operating principles of the proposed system are first introduced from the perspective of adjusting the number of receivers and switching between CC and CV modes. Then, the design and construction of an experimental prototype of the proposed system with two receivers are described. The performance of the system is evaluated for each receiver to assess the performance in both the CV and CC modes and quantify the overall system efficiency.

II. System Modeling

A. System Topology

The multioutput isolated power supply system based on magnetic coupling resonance (MOIPS-MCR) system proposed in this letter is illustrated in Fig. 1(a). It consists of a transmitter

Received 3 June 2024; revised 7 July 2024 and 28 July 2024; accepted 12 August 2024. Date of publication 15 August 2024; date of current version 7 October 2024. *(Corresponding author: Longyang Wang.)*

Jiangui Li, Yinchong Peng, Zheyuan Guo, Guangbin Luo, and Qinghe Si are with the School of Mechanical and Electronic Engineering, Wuhan University of Technology, Wuhan 430070, China (e-mail: jianguili@whut.edu.cn; 283739@whut.edu.cn; guozheyuan@whut.edu.cn; guangbinluo@whut.edu.cn; qinghesi@whut.edu.cn).

Longyang Wang is with the College of Mechanical and Electronic Engineering, China University of Petroleum (East China), Qingdao 266580, China (e-mail: wanglongyang@whut.edu.cn).

Ian Robertson is with the School of Electronic and Electrical Engineering, University of Leeds, LS2 9JT Leeds, U.K. (e-mail: i.d.robertson@leeds.ac.uk).

Color versions of one or more figures in this article are available at https://doi.org/10.1109/TPEL.2024.3444270.

Digital Object Identifier 10.1109/TPEL.2024.3444270

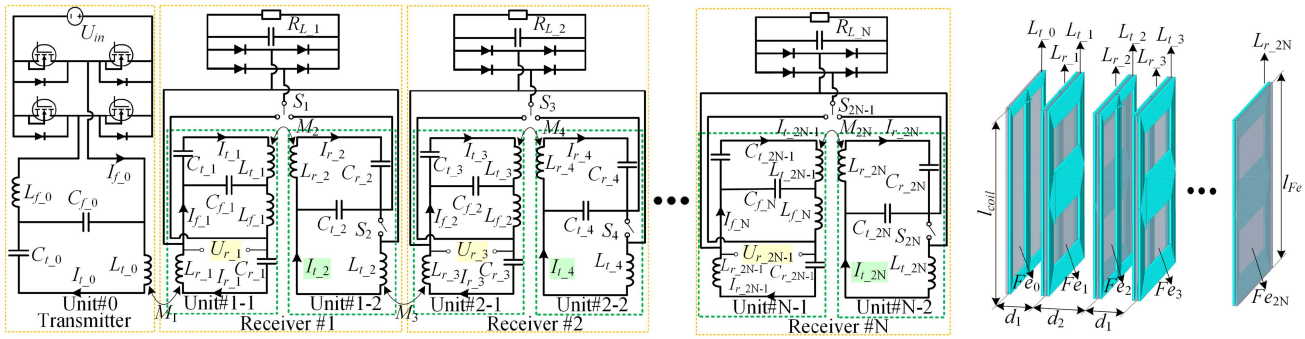

Fig. 1. Proposed topology of the MOIPS-MCR system and the structure of the coupling coils. (a) Proposed topology of the MOIPS-MCR system. (b) Structure of the coupling coils.

unit (Unit #0) and multiple receivers (Receiver #n, $n = 1, 2, \ldots, N$).

The transmitter unit includes a dc power source U_{in}, an inverter, an *LCC* compensation network, and the transmitter coil L_{t_0}. The *LCC* compensation network at the transmitter comprises the inductor L_{f_0} and capacitors C_{f_0} and C_{t_0}.

The nth receiver (Receiver #n) is composed of two units (Unit#n-1 and Unit#n-2), switches S_{2n-1} and S_{2n}, an uncontrolled rectifier, a capacitor filter, and a load R_{L_n}. In Unit#n-1 ($n = 1, 2, \ldots, N-1$), there are two coils, namely, L_{r_2n-1} and L_{t_2n-1}, receiving power from the previous unit and transmitting power to the next unit, respectively. The compensation capacitor C_{r_2n-1} is in series with L_{r_2n-1}, forming an *LCC-S* compensation topology with the previous unit. L_{f_n}, C_{f_n}, and C_{t_2n-1} constitute the *LCC* circuit to compensate L_{t_2n-1}.

In Unit#n-2 ($n = 1, 2, \ldots, N-1$), there are also two coils, namely, L_{r_2n} and L_{t_2n}, receiving power from the previous unit and transmitting power to the next unit, respectively. In addition, L_{t_2n}, C_{t_2n}, and C_{r_2n} form an *LCC* compensation circuit to compensate L_{r_2n}, thereby forming an *LCC–LCC* topology with the previous unit. It is worth noting that the last receiver unit (Unit#N-2) is essentially the same as the previous receiver unit (Unit#(N-1)-2), except that L_{t_2N} no longer serves as the transmitter coil to transfer power.

The mutual inductance between coils L_{t_2n-2} and L_{r_2n-1} is denoted as M_{2n-1} with a coupling coefficient of k_{2n-1}, while the mutual inductance between coils L_{t_2n-1} and L_{r_2n} is denoted as M_{2n} with a coupling coefficient of k_{2n}. The values of k_{2n-1} and k_{2n} can be obtained as

$$\begin{cases} k_{2n-1} = \dfrac{M_{2n-1}}{\sqrt{L_{t\_2n-2}L_{r\_2n-1}}} \\ k_{2n} = \dfrac{M_{2n}}{\sqrt{L_{t\_2n-1}L_{r\_2n}}} \end{cases}, \quad n = 1, 2, \ldots, N. \tag{1}$$

When calculating the mutual inductance, it should be noted that only the mutual inductance between coils L_{t_2n-2} and L_{r_2n-1} and the mutual inductance between coils L_{t_2n-1} and L_{r_2n} should be considered. The mutual inductance between other coils was not considered and was minimized as much as possible in the design process.

B. Coil Design

Based on the aforementioned discussion, the orthogonal structure coils are adopted in this letter to suppress the undesirable cross coupling [8].

Fig. 1(b) illustrates the structure of the coupling coils in the MOIPS-MCR system. The distance between Unit#n-1 and Unit#n-2 and the distance between the transmitter Unit#0 and the Receiver #1's Unit#1-1 are set to $d_1 = 25$ mm. The distance, d_2, between Unit#n-2 and Unit#(n+1)-1 is set to 35 mm. All the coils except L_{f_n} are squares of the same size, with a side length of $l_{\text{coil}} = 150$ mm. The coils L_{t_2n-2} and L_{r_2n-1} share the same structure, with a turn count of $n_1 = 5$ turns. Similarly, the coils L_{t_2n-1} and L_{r_2n} also share the identical structure, with a turn count of $n_2 = 10$ turns. The ferrite plates (Fe_n) are also square with a side length of $l_{\text{Fe}} = 150$ mm.

C. System Analysis

To analyze the CV and CC output characteristics, a function is defined as follows:

$$\text{sgn}(S) = \begin{cases} 0, & S_{2n-1} \text{ is toggled left and } S_{2n} \text{ is switched ON} \\ 1, & S_{2n-1} \text{ is toggled right and } S_{2n} \text{ is switched OFF} \end{cases}. \tag{2}$$

In the proposed system, the compensation inductors and capacitors are designed to fulfill the following condition:

$$\begin{aligned} \omega^2 &= \frac{1}{L_{f\_0}C_{f\_0}} = \frac{1}{(L_{t\_0} - L_{f\_0})C_{t\_0}} = \frac{1}{L_{r\_2n-1}C_{r\_2n-1}} \\ &= \frac{1}{L_{t\_2n}C_{t\_2n}} = \frac{1}{L_{f\_n}C_{f\_n}} = \frac{1}{(L_{t\_2n-1} - L_{f\_n})C_{t\_2n-1}} \\ &= \frac{1}{(L_{r\_2n} - L_{t\_2n})C_{r\_2n}}, \quad n = 1, 2, 3, \ldots, N. \end{aligned} \tag{3}$$

TABLE I
OUTPUT CURRENT AND VOLTAGE OF EACH RECEIVER AT DIFFERENT SWITCH STATES

The state of switches	The voltage or current of Receiver #n (n = 1, 2, 3,⋯, N)			
	Receiver #1	Receiver #2	⋯	Receiver #N
$S_{2n\text{-}1}$ is toggled left, S_{2n} is switched on	$U_{r\_1}=\frac{U_p M_1}{L_{f\_0}}$	$U_{r\_3}=\frac{M_2 M_3}{L_{f\_1} L_{t\_2}} U_{r\_1}$	⋯	$U_{r\_2N-1}=\frac{M_{2N-2} M_{2N-1}}{L_{f\_N-1} L_{t\_2N-2}} U_{r\_2N-3}$
$S_{2n\text{-}1}$ is toggled right, S_{2n} is switched off	$I_{t\_2}=\frac{M_1 M_2 U_p}{j\omega L_{f\_0} L_{f\_1} L_{t\_2}}$	$I_{t\_4}=\frac{M_3 M_4}{L_{f\_2} L_{t\_4}} I_{t\_2}$	⋯	$I_{t\_2N}=\frac{M_{2N-1} M_{2N}}{L_{f\_N} L_{t\_2N}} I_{t\_2N-2}$

According to the coil structure in Section II-B, the following constraints can be derived:

$$\begin{cases} L_{t\_0}=L_{r\_1}=L_{t\_2}=L_{r\_3}=\cdots=L_{t\_2N-2}=L_{r\_2N-1} \\ L_{t\_1}=L_{r\_2}=L_{t\_3}=L_{r\_4}=\cdots=L_{t\_2N-1}=L_{r\_2N} \\ M_1=M_3=\cdots=M_{2N-1}, k_1=k_3=\cdots=k_{2N-1} \\ M_2=M_4=\cdots=M_{2N}, k_2=k_4=\cdots=k_{2N} \end{cases}. \tag{4}$$

According to Kirchhoff's voltage law, (5) can then be derived.

To simplify the analysis, the parasitic resistance of the inductors is ignored. By substituting (3) into (5), the load voltage $U_{r\_2n\text{-}1}$ or load current I_{t_2n} in Receiver #n can be derived, as given in Table I.

According to Table I, when switch $S_{2n\text{-}1}$ is toggled left and S_{2n} is switched ON, the output voltage $U_{r\_2n\text{-}1}$ at each receiver is independent of the load. Conversely, when switch $S_{2n\text{-}1}$ is toggled right and S_{2n} is switched OFF, the output current I_{t_2n} at each receiver is independent of the load. Moreover, it can be found that the receivers added later do not affect the output state of the existing receivers, so the flexible adjustment of the number of receivers can be achieved. When each receiver operates in CV mode or CC mode and the condition shown in (6) is satisfied, equal output voltages or equal output currents can be obtained

$$\begin{cases} U_p=j\omega L_{f\_0} I_{f\_0}+(I_{f\_0}-I_{t\_0})\frac{1}{j\omega C_{f\_0}} \\ 0=-(I_{f\_0}-I_{t\_0})\frac{1}{j\omega C_{f\_0}}+I_{t\_0}(j\omega L_{t\_0}+\frac{1}{j\omega C_{t\_0}}) \\ \quad -j\omega M_1 I_{r\_1} \\ 0=-j\omega M_{2n-1} I_{t\_2n-2}+I_{r\_2n-1}(j\omega L_{r\_2n-1} \\ \quad +\frac{1}{j\omega C_{r\_2n-1}})+U_{r\_2n-1} \\ 0=-U_{r\_2n-1}+j\omega L_{f\_n} I_{f\_n}+(I_{f\_n}-I_{t\_2n-1})\frac{1}{j\omega C_{f\_n}} \\ 0=-(I_{f\_n}-I_{t\_2n-1})\frac{1}{j\omega C_{f\_n}}+I_{t\_2n-1}\frac{1}{j\omega C_{t\_2n-1}} \\ \quad +j\omega L_{t\_2n-1} I_{t\_2n-1}-j\omega M_{2n} I_{r\_2n} \\ 0=I_{r\_2n}(j\omega L_{r\_2n}+\frac{1}{j\omega C_{r\_2n}})+(I_{r\_2n}-I_{t\_2n})\frac{1}{j\omega C_{t\_2n}} \\ \quad -j\omega M_{2n} I_{t\_2n-1} \\ 0=-j\omega M_{2m+1} I_{r\_2m+1}+\mathrm{sgn}(S) I_{t\_2m} R_{E\_m} \\ \quad +j\omega L_{t\_2m} I_{t\_2m}-(I_{r\_2m}-I_{t\_2m})\frac{1}{j\omega C_{t\_2m}}, \\ \quad m=1,2,\ldots,N-1 \\ 0=-(I_{r\_2N}-I_{t\_2N})\frac{1}{j\omega C_{t\_2N}}+\mathrm{sgn}(S) I_{t\_2N} R_{E\_N} \\ \quad +j\omega L_{t\_2N} I_{t\_2N} \end{cases} \tag{5}$$

where n = 1, 2, …, N, U_p is the equivalent sinusoidal voltage source, R_{E_n} is the equivalent ac impedance, and the definition of $U_{r\_2n\text{-}1}$ is given in Fig. 1(a)

$$\begin{cases} M_1=M_3=\cdots=M_{2N-1}=L_{f\_0}=L_{f\_1}=\cdots=L_{f\_N} \\ M_2=M_4=\cdots=M_{2N}=L_{t\_0}=L_{t\_2}=\cdots=L_{t\_2N} \end{cases}. \tag{6}$$

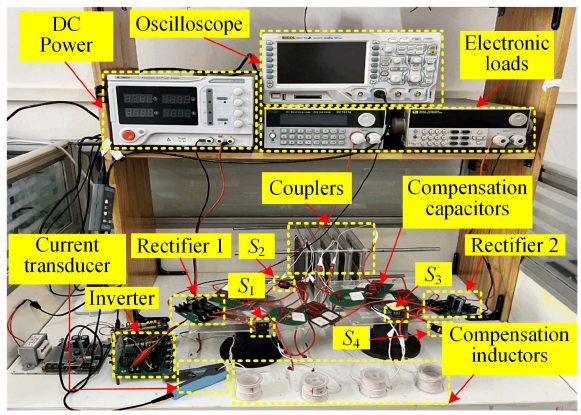

Fig. 2. Experimental platform with two receivers.

TABLE II
MAIN PARAMETERS OF THE EXPERIMENTAL PLATFORM

Symbol	Value	Symbol	Value
U_{in}	36 V	f	300 kHz
C_{t_0}	19 924 pF	L_{t_4}	28.5 μH
L_{f_0}–L_{f_3}	13.5 μH	C_{f_0}–C_{f_3}	23121 pF
C_{r_1}, C_{r_3}	10 294 pF	C_{r_2}, C_{r_4}	7305 pF
C_{t_1}, C_{t_3}	5236 pF	C_{t_2}, C_{t_4}	10116 pF
L_{t_0}–L_{r_1}	28.5 μH	L_{t_1}–L_{r_2}	66.5 μH
L_{t_2}–L_{r_3}	28.5 μH	L_{t_3}–L_{r_4}	66.5 μH

The output power of Receiver #n can be obtained as

$$P_n=\begin{cases} \frac{U_{r\_2n-1}^2}{R_{E\_n}}, & \mathrm{sgn}(S)=0 \\ I_{t\_2n}^2 R_{E\_n}, & \mathrm{sgn}(S)=1 \end{cases}. \tag{7}$$

The total output power and transmission efficiency of the proposed system with n ($n=1,2,\ldots,N$) receivers can be derived as

$$\begin{cases} P_{\mathrm{OUT}}=\sum_{n=1}^{N} P_n \\ P_{\mathrm{IN}}=|U_{\mathrm{in}} I_{f\_0}| \\ \eta=\frac{P_{\mathrm{OUT}}}{P_{\mathrm{IN}}} \end{cases}. \tag{8}$$

III. EXPERIMENTAL VALIDATION

A. Experimental System Setup

For the validation of the voltage or current characteristics of the MOIPS-MCR system, an experimental platform with two receivers ($N=2$) was constructed, as shown in Fig. 2. The main parameters of the practical system are listed in Table II.

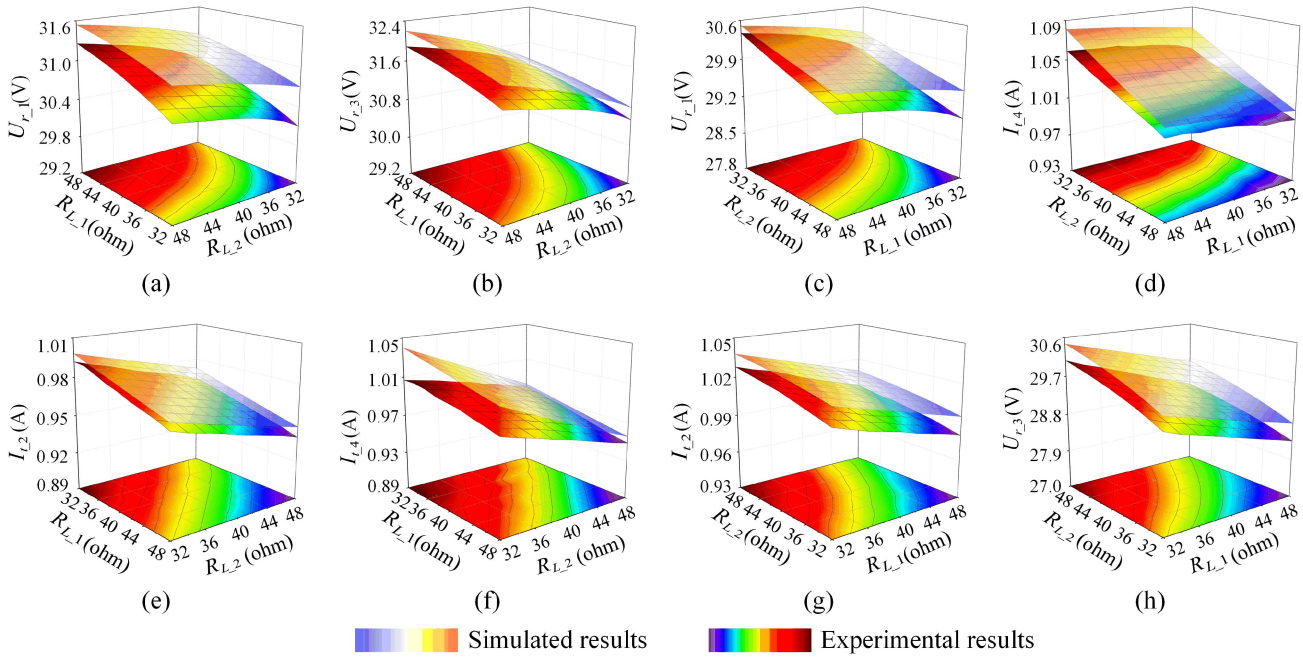

Fig. 3. Simulated and experimental output voltage and current against the load variations. (a) First receiver output voltage under mode A. (b) Second receiver output voltage under mode A. (c) First receiver output voltage under mode B. (d) Second receiver output current under mode B. (e) First receiver output current under mode C. (f) Second receiver output current under mode C. (g) First receiver output current under mode D. (h) Second receiver output voltage under mode D.

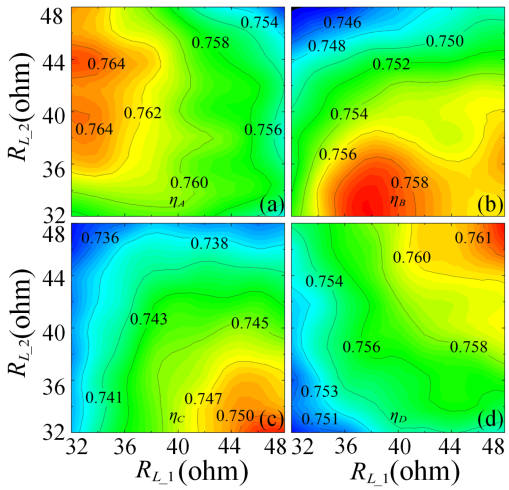

Fig. 4. System efficiency in different operating modes. (a) Mode A. (b) Mode B. (c) Mode C. (d) Mode D.

B. Experimental Results and Analysis

To validate the effectiveness of CC or CV performance of each receiver, the current and voltage were measured as a function of the load resistance. The proposed system with two receivers can operate in four operational modes: A, B, C, and D. In mode A, both Receiver #1 and Receiver #2 operate in the CV mode. In mode B, Receiver #1 operates in the CV mode, while Receiver #2 operates in the CC mode. In mode C, both Receiver #1 and Receiver #2 operate in the CC mode. In mode D, Receiver #1 operates in the CC mode, while Receiver #2 operates in the CV mode.

The variations in voltage or current obtained from simulation and experiment for each receiver of the system under the four operational modes (A, B, C, and D) are shown in Fig. 3. From Fig. 3(a), (b), (c), and (h), when the loads R_{L_1} and R_{L_2} vary from 32 to 48 Ω in modes A, B, and D, both the output voltage U_{r_1} of the first receiver and the output voltage U_{r_3} of the second receiver exhibit excellent CV characteristics. Fig. 3(d)–(g) demonstrates that both the output current I_{t_2} of the first receiver and the output current I_{t_4} of the second receiver exhibit excellent CC characteristics when the loads R_{L_1} and R_{L_2} vary from 32 to 48 Ω in modes B, C, and D. The slight fluctuations in the output voltage or current may be attributed to the parasitic resistance of the coupling coils and the parasitics of the compensation components. The simulated and experimental voltages and currents have the same trend with load variations. Moreover, the experimental voltages and currents agree well with the simulated results, and the simulated values are slightly larger than the experimental values. The differences are mainly caused by manufacturing errors of the coupler and compensation components and measurement errors.

The efficiency of the system in the four operating modes is shown in Fig. 4. It is evident that the system efficiency in all four operating modes is above 73%, with the maximum efficiency being 76.6%. This is achieved when the system operates in mode A with total output power being 51.22 W, corresponding to a first receiver load R_{L_1} of 32 Ω and a second receiver load R_{L_2} of 44 Ω.

Fig. 5 illustrates the experimental voltage and current waveforms. When R_{L_1} and R_{L_2} are set to 32 Ω, the output voltage U_{inv} and current I_{f_0} of the inverter under mode C and the output voltage before the rectifier of the two receivers under mode A

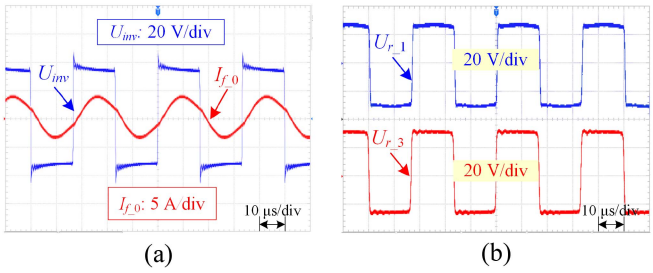

Fig. 5. Experimental voltage and current waveforms. (a) Output voltage and current of the inverter. (b) Output voltage of Receiver #1 and Receiver #2.

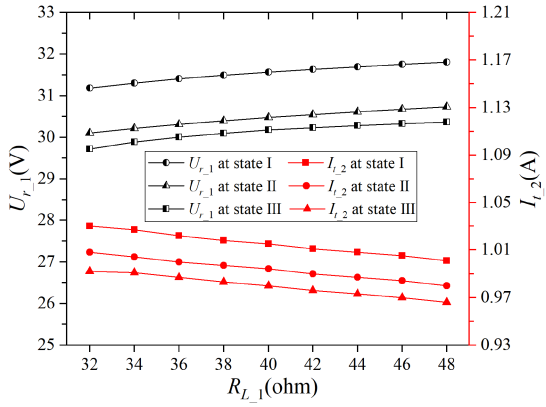

Fig. 6. Output voltage U_{r_1} and current I_{t_2} of Receiver #1 in three different states.

are presented in Fig. 5(a) and (b), respectively. As can be seen from Fig. 5(a), the output voltage and current of the inverter are almost in phase. It is evident from Fig. 5(b) that the output voltages of the two receivers are in phase, and their amplitudes are nearly identical.

To validate the conclusion that adding additional receivers does not affect the output state of the existing receivers, the voltage U_{r_1} and the current I_{t_2} were measured as a function of the load resistance of R_{L_1} when the system operates in three states. In state I, only Receiver #1 works. In state II, Receiver #1 works when Receiver #2 operates in the CV mode, with R_{L_2} being 32 Ω. In state III, Receiver #1 works when Receiver #2 operates in the CC mode, with R_{L_2} being 32 Ω. In the aforementioned three states, Receiver #1 works in two modes, i.e., CV and CC modes, and the load resistance of R_{L_1} varies from 32 to 48 Ω.

Fig. 6 shows the variation of voltage and current of Receiver #1 in three states. When the system operates in state III, the output voltage U_{r_1} is about 4.49% smaller than that in state I, and the output current I_{t_2} is about 3.49% smaller than that in state I. When the system operates in state II, the output voltage U_{r_1} is about 3.44% smaller than that in state I, and the output current I_{t_2} is about 2.14% smaller than that in state I. It can be observed that the voltage and current drops are relatively small and within the acceptable limits when Receiver #2 is connected into the system.

IV. Conclusion

This letter proposes a multioutput isolated power supply system based on magnetic coupling resonance wireless power transmission technology. It can be utilized to simultaneously power multiple devices, with CV or CC mode being selected by toggling switches to different states. An experimental demonstration of the MOIPS-MCR system with two receivers was produced to validate the proposed technique. Experimental results demonstrate that the load-independent CV or CC output mode can be achieved over a wide range of load resistance, and the system efficiency is all above 73%. Moreover, the adding of additional receivers does not affect the output state of the existing receivers, so the flexible adjustment of the number of receivers can be achieved.

References

[1] J. Zhang, J. Liu, J. Yang, N. Zhao, Y. Wang, and T. Q. Zheng, "A modified DC power electronic transformer based on series connection of full-bridge converters," *IEEE Trans. Power Electron.*, vol. 34, no. 3, pp. 2119–2133, Mar. 2019.

[2] E. Serban, M. A. Saket, and M. Ordonez, "High-performance isolated gate-driver power supply with integrated planar transformer," *IEEE Trans. Power Electron.*, vol. 36, no. 10, pp. 11409–11420, Oct. 2021.

[3] L. Wang, J. Li, H. Chen, and Z. Pan, "Radial-flux rotational wireless power transfer system with rotor state identification," *IEEE Trans. Power Electron.*, vol. 37, no. 5, pp. 6206–6216, May 2022.

[4] C. Cai et al., "Hybrid interference field mitigation of dual-rectangular transmitter pad for universal wireless charging area expansion," *IEEE Trans. Transp. Electrific.*, vol. 10, no. 2, pp. 3816–3827, Jun. 2024, doi: 10.1109/TTE.2023.3307233.

[5] C. Cai et al., "Optical fiber composite winding for in situ thermal monitoring of transmitter magnetic mechanism in long-track DWPT systems," *IEEE Trans. Instrum. Meas.*, vol. 73, 2024, Art. no. 9000604.

[6] Y. Li, J. Hu, X. Li, and K.-W. E. Cheng, "A flexible load-independent multi-output wireless power transfer system based on cascaded double T-resonant circuits: Analysis, design and experimental verification," *IEEE Trans. Circuits Syst. I: Reg. Papers*, vol. 66, no. 7, pp. 2803–2812, Jul. 2019.

[7] X. He, C. Zhu, J. Tao, Y. Zhang, and R. Mai, "Analysis and design of a cost-effective WPT system with single-input and multioutput based on buck-integrated rectifier," *IEEE Trans. Power Electron.*, vol. 38, no. 10, pp. 12388–12393, Oct. 2023.

[8] C. Cheng, W. Li, Z. Zhou, Z. Deng, and C. Mi, "A load-independent wireless power transfer system with multiple constant voltage outputs," *IEEE Trans. Power Electron.*, vol. 35, no. 4, pp. 3328–3331, Apr. 2020.

[9] C. Cheng, Z. Zhou, W. Li, C. Zhu, Z. Deng, and C. C. Mi, "A multi-load wireless power transfer system with series-parallel-series compensation," *IEEE Trans. Power Electron.*, vol. 34, no. 8, pp. 7126–7130, Aug. 2019.

[10] C. Cheng et al., "A load-independent LCC-compensated wireless power transfer system for multiple loads with a compact coupler design," *IEEE Trans. Power Electron.*, vol. 67, no. 6, pp. 4507–4515, Jun. 2020.